nature geoscience

Article

https://doi.org/10.1038/s41561-023-01331-y

Local cooling and drying induced by Himalayan glaciers under global warming

Received: 19 December 2022

Accepted: 20 October 2023

Published online: 04 December 2023

Check for updates

Franco Salerno[1,2,18] ✉, Nicolas Guyennon[3,18] ✉, Kun Yang[4,5], Thomas E. Shaw[6,7], Changgui Lin[8], Nicola Colombo[3,9], Emanuele Romano[3], Stephan Gruber[10], Tobias Bolch[11], Andrea Alessandri[12], Paolo Cristofanelli[12], Davide Putero[13], Guglielmina Diolaiuti[14], Gianni Tartari[2], Gianpietro Verza[15], Sudeep Thakuri[16], Gianpaolo Balsamo[17], Evan S. Miles[6] & Francesca Pellicciotti[6,7]

Understanding the response of Himalayan glaciers to global warming is vital because of their role as a water source for the Asian subcontinent. However, great uncertainties still exist on the climate drivers of past and present glacier changes across scales. Here, we analyse continuous hourly climate station data from a glacierized elevation (Pyramid station, Mount Everest) since 1994 together with other ground observations and climate reanalysis. We show that a decrease in maximum air temperature and precipitation occurred during the last three decades at Pyramid in response to global warming. Reanalysis data suggest a broader occurrence of this effect in the glacierized areas of the Himalaya. We hypothesize that the counterintuitive cooling is caused by enhanced sensible heat exchange and the associated increase in glacier katabatic wind, which draws cool air downward from higher elevations. The stronger katabatic winds have also lowered the elevation of local wind convergence, thereby diminishing precipitation in glacial areas and negatively affecting glacier mass balance. This local cooling may have partially preserved glaciers from melting and could help protect the periglacial environment.

Himalayan glaciers have been losing mass consistently, with an acceleration in the last five decades, including at the iconic Mount Everest[1–3]. Whereas the increase in temperature over the last decades is recognized as a first-order control on melting[4], how glaciers modulate the local climate remains unknown, also because of limited high-elevation stations[5]. This challenges both our understanding of ongoing changes and modelling skills to anticipate future changes[6].

Here, we investigate the non-stationarity of the Himalayan climate (temperature, precipitation and wind) during the last three decades from the hourly to the seasonal scale. We use all existing daily

[1]National Research Council, Institute of Polar Sciences, ISP-CNR, Milan, Italy. [2]National Research Council, Water Research Institute, IRSA-CNR, Brugherio, MB, Italy. [3]National Research Council, Water Research Institute, IRSA-CNR, Montelibretti, Roma, Italy. [4]Ministry of Education Key Laboratory for Earth System Modeling, Department of Earth System Science, Tsinghua University, Beijing, China. [5]National Tibetan Plateau Data Center, State Key Laboratory of Tibetan Plateau Earth System and Resource Environment, Institute of Tibetan Plateau Research, Chinese Academy of Sciences, Beijing, China. [6]Swiss Federal Institute for Forest, Snow and Landscape Research, Birmensdorf, Switzerland. [7]Institute of Science and Technology Austria, ISTA, Klosterneuburg, Austria. [8]National Space Science Center, Chinese Academy of Sciences, Beijing, China. [9]Department of Agricultural, Forest and Food Sciences, University of Turin, Grugliasco, Italy. [10]Carleton University, Department of Geography and Environmental Studies, Ottawa, Canada. [11]Graz University of Technology, Institute of Geodesy, Graz, Austria. [12]National Research Council, Institute of Atmospheric Sciences and Climate, ISAC-CNR, Bologna, Italy. [13]National Research Council, Institute of Atmospheric Sciences and Climate, ISAC-CNR, Torino, Italy. [14]University of Milan, Department of Environmental Science and Policy, Milan, Italy. [15]Ev-K2-Minoprio, Bergamo, Italy. [16]Central Department of Environmental Science, Tribhuvan University, Kirtipur, Nepal. [17]European Centre for Medium Range Weather Forecasts, Reading, UK. [18]These authors contributed equally: Franco Salerno, Nicolas Guyennon. ✉e-mail: franco.salerno@cnr.it; nicolas.guyennon@irsa.cnr.it

observational climatic time series at high elevation and ERA5-Land reanalysis data. We take advantage of the longest time series of meteorological data at a glacierized elevation in Himalaya, the Pyramid Observatory Laboratory (on the southern slopes of Mount Everest, Nepal, 5,035 m above sea level (a.s.l.), off glacier, hereafter Pyramid$_{off}$) (Supplementary Fig. 1), which has continuously recorded hourly meteorological data since 1994. We also exploit the only five existing long-term climatic time series close to the main Himalayan ridge, located from 3,900 to ~4,500 m a.s.l. (Supplementary Table 1). We explore the physical processes behind the observed climate dynamics using three more stations along the southern slopes of Mount Everest, together with ozone data collected at Pyramid$_{off}$. Building on the agreement between ground observations and ERA5-Land reanalysis data, we extend our findings from Mount Everest to the entire Himalayan range, revealing an unknown picture of high mountain climate in the region.

Cooling trends of diurnal air temperature

In contrast to most regional and global records[7], we find that the mean annual air temperature (T_{mean}) has been stationary at Pyramid$_{off}$ during the last three decades (−0.002 ± 0.009 °C yr^{-1}, $P > 0.1$, 1994–2020 period, Supplementary Table 2 and Supplementary Fig. 2, black line). This unexpected observation seems in contrast with the attribution of the accelerated glacier mass loss to increasing air temperature[8]. To reconcile this apparent discrepancy, we take advantage of the unique climatic dataset at Pyramid$_{off}$ and analyse its diurnal temperature (T_{max}) and nocturnal temperature (T_{min}) separately, partitioning the year into two periods: the cold season from November to April and the warm season from May to October. We find that the T_{mean} trend has been brought to zero by a significant decrease in T_{max} (−0.040 ± 0.020 °C yr^{-1}, $P < 0.01$) during all months of the warm season. This decrease in T_{max} started about 15 years ago (Fig. 1c,d, orange line), in contrast to T_{min}, which has increased consistently, mainly during the cold season (+0.046 ± 0.019 °C yr^{-1}, $P < 0.01$, Supplementary Fig. 3b, blue line). T_{max} exerts a crucial control on both melting processes and katabatic wind generation, when T_{max} is generally above +0 °C, while T_{min} is mainly negative during the cold season and remains so despite the increase. Therefore, we focus on the non-stationarity of T_{max}, which is the key control of glacier melt and its sensitivity to warming.

We find negative T_{max} trends at all the other existing stations close to the Himalayan glaciers: a similar trend exists at Pheriche$_{off}$ (4,260 m a.s.l.), in the same valley as Pyramid$_{off}$, which also excludes instrumental errors at single sites (Supplementary Fig. 4a); and negative T_{max} trends occur at all the southernmost stations on the Tibetan Plateau[9], mainly at the beginning of the warm season (May to July) (Supplementary Fig. 5, location in Fig. 1a). The stations with weaker declines in T_{max} are farther from the glaciers than Pyramid$_{off}$. The consistency of the cooling trends across all available high-elevation stations lends confidence that this is a process typical of Himalayan glacierized regions beyond the Everest region.

Crucially, we find that the overall decreasing T_{max} trend at Pyramid$_{off}$, particularly during the warm season, is correctly reproduced by ERA5-Land reanalysis (−0.026 ± 0.014 °C yr^{-1}, $P < 0.05$, Fig. 1e,f), which reproduces the non-stationary patterns at the annual and monthly scale (Fig. 1c).

Regional cooling associated with the glacier mass

Given the correspondence between observations and reanalysis at Pyramid$_{off}$, we explore the warm season T_{max} trend across the entire Himalaya (75° E to 91° E) based on ERA5-Land (Fig. 1a). The region includes glaciers that accumulate snow primarily during winter (predominantly in western Himalaya) and during the summer monsoon (eastern Himalaya) but are homogeneous from a morphometric point of view[10]. To describe the regional trends, we split the transect into four subregions (Lahaul-Spiti, Western, Central and Eastern Himalaya)[3].

In agreement with the Pyramid$_{off}$ record, a decrease in T_{max} is evident in the entire region over the glacier surfaces (Fig. 1a). A similar pattern of decreasing trends is observed for T_{mean} (Supplementary Figs. 2, 3, 6 and 7). The decrease in T_{max} is particularly strong in Lahaul-Spiti and in Central-Eastern Himalaya, characterized by the largest ice masses, and is less strong in Western Himalaya, where glaciers are less abundant[8,11] (Fig. 1a).

Whereas an elevation-dependent warming (that is, stronger warming rate at higher elevations) has been suggested at the global level[6], we find that glaciers are associated with a significant reduction of the local warming. In non-glacial conditions, we also observe a direct elevation-dependent warming, in particular above 4,000 m a.s.l. (up to +0.05 °C yr^{-1}) (Fig. 1b). Cooling trends (up to −0.05 °C yr^{-1}), however, are evident at all glacierized locations (black points in Fig. 1b) ($P < 0.001$ for the analysis of variance test on the means). At lower elevations, trends are positive, although less strong (mean +0.023 °C yr^{-1}, $P < 0.1$) than those found at higher, non-glacierized elevations. The magnitude of the low-elevation trends in ERA5-Land corresponds well with the trend that we observe at 27 ground stations in Nepal below 2,000 m a.s.l. (mean +0.026 °C yr^{-1}, $P < 0.01$, Supplementary Fig. 8).

Negative trends in T_{max} are associated with glacier masses consistently across reanalysis and all available observations (Supplementary Fig. 5a–c). The smaller time window over which a trend is evident (beginning of the warm season) is probably due to a smaller influence of glaciers induced by the reduced extension of glacial masses and the larger minimum distance from the glacier fronts in the station surroundings (Supplementary Table 1 and Supplementary Fig. 9). On the contrary, we find no clear T_{max} trends in the warm season (Supplementary Fig. 5d,e) for those stations without glaciers within a 20 km radius (Supplementary Table 1 and Supplementary Fig. 9).

Conceptual model of cooling and drying

The unexpected finding of cooling at high elevation close to glacier masses requires revisiting our understanding of glacier–atmosphere interactions. In the ablation season, the free atmosphere temperature (T_{fa}) on midlatitude glaciers is typically higher than the glacier surface temperature (T_s), which is close to 0 °C, since the excess energy at the ice surface is used for melting (Fig. 2a)[12].

Katabatic winds arise from adiabatic warming due to air subsidence and cooling of the near-surface air by sensible heat exchange with the glacier surface[13]. The interplay of these processes lowers the 2 m on-glacier temperature (T_g) (the so-called glacier cooling effect)[14,15] giving rise to density gradients that drive the air down glacier.

Katabatic winds draw air masses from upper regions[16] and we postulate an air convergence over upper parts of these glaciers, where strong air exchanges with higher atmospheric layers may occur[17]. This process generates a divergence of air masses along the northern and southern Himalayan valleys and causes further drying of the katabatic winds.

The variations of T_g along the glacier flowline are complex to model[14,18]. A growing body of studies, however, has shown stronger cooling effects at greater flow distances, until a maximum cooling point (from I_0 to II_0 in Fig. 2a)[16]. This point can be followed by an increase in temperature over the glacier tongues (III_0 in Fig. 2a)[18] due to up-valley afternoon winds[19] counterbalancing the cooling effect of katabatic winds[18]. Recently, ref. 20 postulated that these moist, upward air masses counteract the cool, downwards katabatic winds, creating a local convergence. This process can force the warm and moist monsoonal air masses to uplift, inducing precipitation to occur near to, or below, the glacier fronts.

During non-stationary conditions, as in a global warming phase (Fig. 2b), higher free atmosphere temperature induces higher sensible heat exchange between the glacier surface and the

https://doi.org/10.1038/s41561-023-01331-y

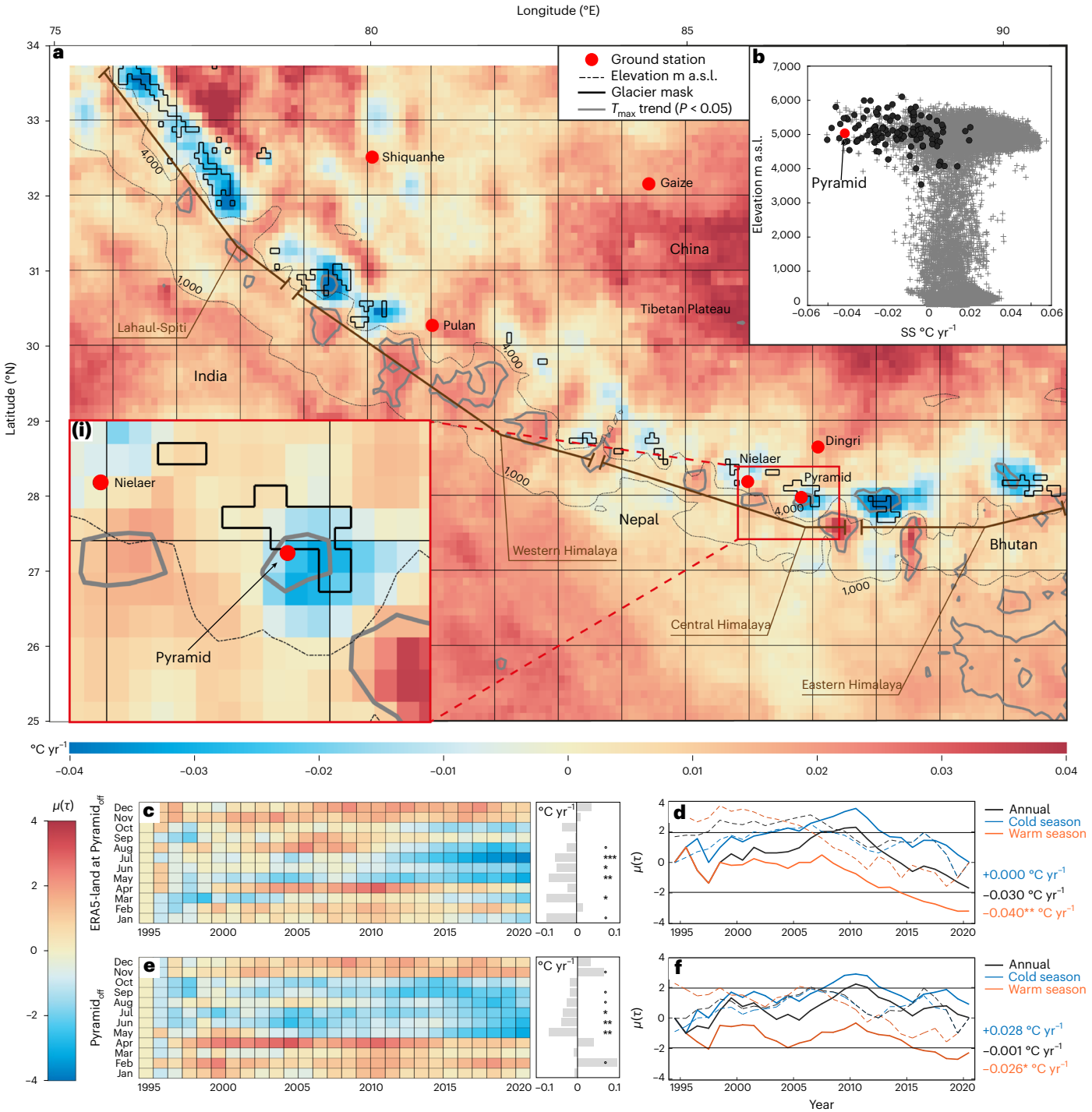

Fig. 1 | Trend analysis for maximum 2 m air temperature in Himalaya during 1994–2020. a, Himalayan trend of ERA5-Land T_{max} referred to the warm season (1994–2020). The map shows the location of the observational air temperature time series and the glacier mask used in ERA5-Land. Cold and warm colours represent decreasing and increasing trends, respectively, with associated Mann–Kendall (MK) test significance. The insert (i) provides a better picture of the ERA5-Land trends in the surrounding of the analysed ground stations. **b**, Elevation-dependence of T_{max} SS for all cells in **a** (grey). The black points represent the cells located inside the glacier mask. **c**,**e**, Observational data (Pyramid$_{off}$) (**c**) and the correspondent pixel of ERA5-Land (**e**). The grids display the results of the MK test applied at the monthly scale and calculated from the beginning of the series to the given year. The colour bar represents the normalized Kendall's tau coefficient $\mu(\tau)$. The colour tones below −1.96 and above 1.96 are significant (α = 5%). On the right, the monthly Sen's Slope (SS) and the significance levels for 1994–2020 (°P < 0.1, *P < 0.05, **P < 0.01, ***P < 0.001). **d**,**f**, Observational data (Pyramid$_{off}$) (**d**) and the correspondent pixel of ERA5-Land (**f**). The progressive $\mu(\tau)$ (solid lines) and retrograde (dotted line) of the seqMK test (that is, calculated from the beginning or from the end, respectively, of the series to the given year) for the cold season (NDJFMA) (blue), the warm season (MJJASO) (orange) and for the entire year (black). For each year, below-zero lines indicate negative trends (calculated from 1994).

near-surface air. On one hand, the additional heat is used to increase the melting rates, causing enhanced glacier mass losses. On the other hand, a further cooling of the surface air over glaciers generates more intense katabatic winds.

As a key consequence of the increased katabatic winds, the glacier cooling effect intrudes downstream into the periglacial environment, shifting the local convergence between up- and down-valley winds lower (Fig. 2b). Increased dry and cold winds push downwards the

https://doi.org/10.1038/s41561-023-01331-y

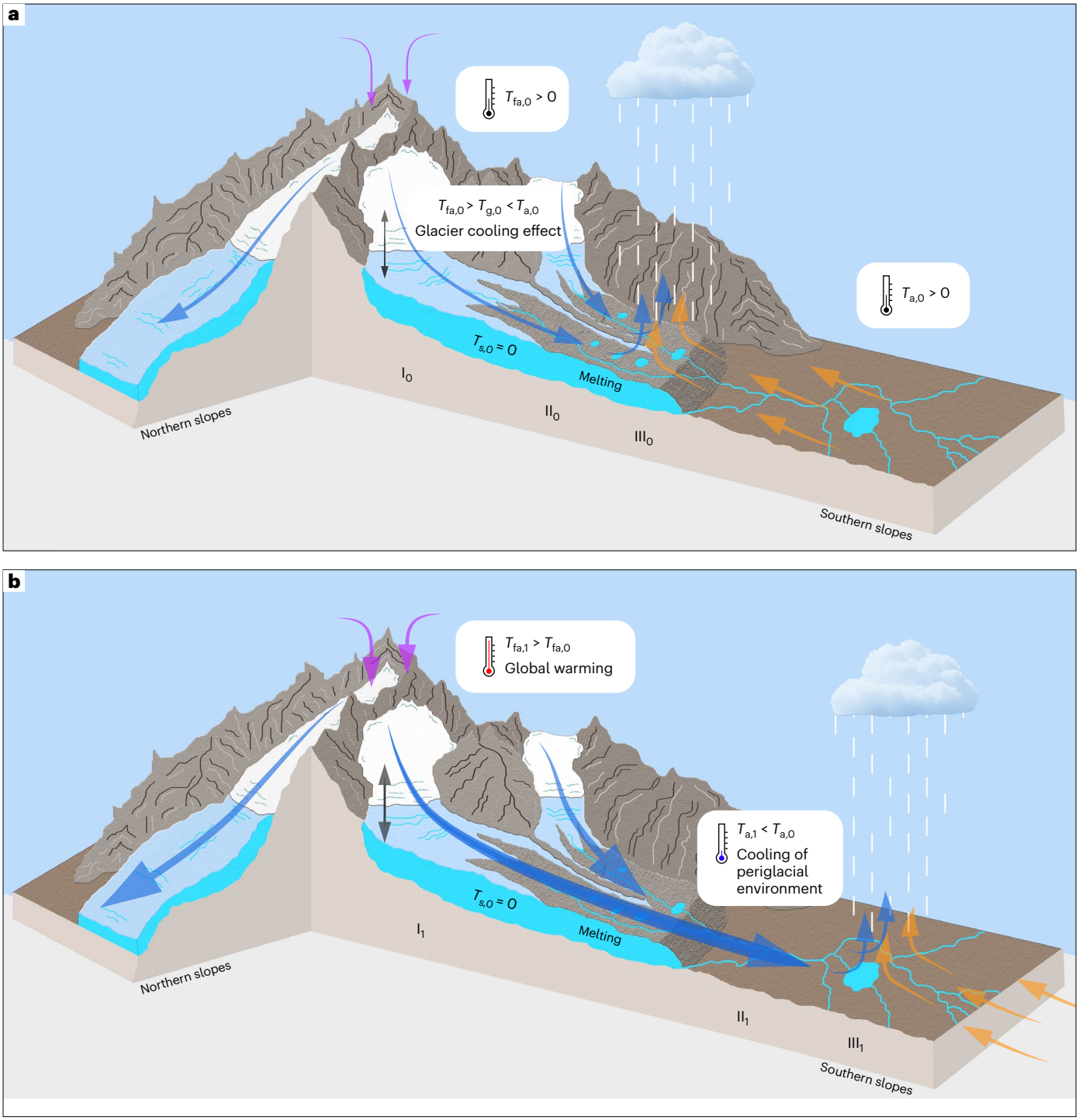

Fig. 2 | Schematic diagrams explaining the air cooling observed in the surroundings of Himalayan glaciers. a,**b**, In both diagrams, an idealized case of wind interactions (vertical, katabatic and up-valley), that potentially dictate the along-flowline structure of on-glacier air temperature, is represented. **a**, Diagram for stationary conditions (subscript 0). Points I, II and III indicate locations of interest: point I_0 represents the glacier zone, where T_g is more similar to T_{fa} and therefore less influenced by the glacier cooling effect; point II_0 is the glacier part, where ideally the cooling is at its maximum; point III_0 is the convergence zone between upward and downward winds, where the upshift of moist air masses induces the occurrence of precipitation. **b**, Diagram for non-stationary conditions (subscript 1). Currently, global warming increases the flux of sensible heat toward the glacier surface and thus enhances the cooling of near-glacier-surface air. Consequently, katabatic winds become more intense and capable of drawing further cold air masses from the higher elevations. As a result, the glacier cooling effect reaches downstream the periglacial environment (from II_0 to II_1), downshifting the convergence zone (from III_0 to III_1). T_s, temperature of glacier surface; T_a, temperature ambient; T_{fa}, temperature of free atmosphere; T_g, 2 m on-glacier temperature.

https://doi.org/10.1038/s41561-023-01331-y

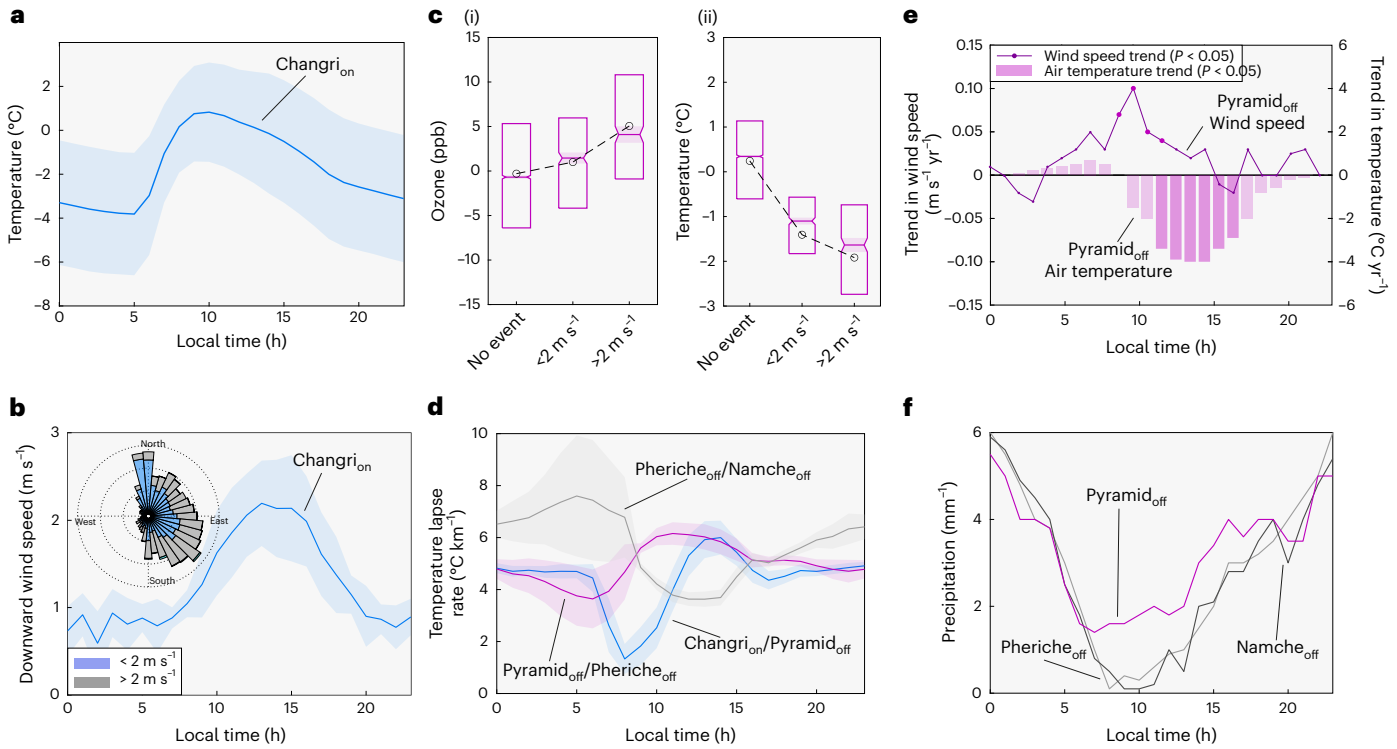

Fig. 3 | Observations during the warm season on the south slopes of Mount Everest. a, Hourly mean of the 2 m air temperature at Changri$_{on}$ (thick line, mean; shadow area, standard deviation of the warm season). **b**, Wind rose and downward wind speed among hours of northerly (90°–270°) flow at Changri$_{on}$ (thick line, hourly mean; shadow area, standard deviation of the warm season). **c**, Boxplots of ozone concentration (n = 8,088, n = 646, n = 390) (i) and air temperature (ii) related to three classes of hourly wind speed at Changri$_{on}$ defined on the basis of the following criteria: wind direction between 90° and 270° (southward) and wind speed >1 m s^{-1}. When one of these criteria was not satisfied, we included the observations in the 'no event' class (n = 7,578, n = 656, n = 395), the centre lines and box limits represent median values, 25th to 75th percentiles, respectively. **d**, Hourly lapse rates between meteorological stations located along the elevation gradient during 2011–2015 (map, Supplementary Fig. 1). A decreasing lapse rate denotes warming at higher elevation or cooling at lower elevation and vice versa. Note that the warming during the early morning at the station at higher elevation (Changri$_{on}$/Pyramid$_{off}$ at 9:00) is due to the different timing of exposure to solar radiation[22]. **e**, Trend analysis (1994–2020) of hourly downward wind speed (hollow) and air temperature (solid) at Pyramid$_{off}$. **f**, Hourly mean precipitation at the ground stations (ref. 20, revised).

water vapour transported by the summer monsoon reducing moisture supply for precipitation over the upper parts of glaciers and thus reducing glacier accumulation.

Observations supporting the conceptual model

Measurements at the off-glacier stations downstream of Pyramid$_{off}$, Pheriche$_{off}$ (4,260 m a.s.l.) and Namche$_{off}$ (3,570 m a.s.l.) and at the on-glacier Changri-Nup (Changri$_{on}$, 5,700 m a.s.l.) (Supplementary Table 3 and Supplementary Fig. 1; Methods) provide the observational evidence for our model (Fig. 2).

During the warm season, the mean 2 m air temperature recorded on glaciers is above 0 °C from 9:00 to 13:00 (local time) at Changri$_{on}$ (Fig. 3a), a condition favourable for the exchanging of sensible heat, which in turn allows the development of katabatic winds. As a result, from the early morning (9:00) the katabatic winds flow downward reaching the maximum speed during the first hours of the afternoon and decreasing in the evening (Fig. 3b), when the upward winds prevail[19].

The exchange of air masses between the upper atmospheric layers and the glacier surface can be inferred from ozone (O_3) data[17,21]. We find significantly higher ozone concentrations in correspondence to stronger downward winds at Pyramid$_{off}$ (Fig. 3c1). When katabatic winds are stronger, temperatures are lower at Pyramid$_{off}$ (Fig. 3c2), suggesting that air masses are drawn from the surrounding high-elevation reaches of the glaciers. This suggests that, during daytime, stronger katabatic winds are capable of transporting downward O_3-rich air masses from high elevations to the glacier surfaces and the proglacial domain (Pyramid$_{off}$).

The diurnal down-glacier lowering of temperature is evident when analysing how the relationship between temperature and elevation varies during the day (Fig. 3d). We find midday lower temperature gradients until 4,260 m a.s.l. (Changri$_{on}$/Pyramid$_{off}$ and Pyramid$_{off}$/Pheriche$_{off}$ show lower temperature gradients between 13:00 and 16:00 and 10:00 and 16:00, respectively), which do not occur downstream at 3,560 m a.s.l. (Pheriche$_{off}$/Namche$_{off}$ shows higher temperature at midday). Note that the higher temperature during the early morning at the station at higher elevation (Changri$_{on}$/Pyramid$_{off}$ at 9:00) is caused by the different timing of exposure to solar radiation[22]. An increase of katabatic winds, explaining the observed downstream cooling trend, is evident in the period of record. At Pyramid$_{off}$, wind speed from the early morning until the first hours of the afternoon increased during 1994–2020, with statistically significant increases from 9:00 to 10:00 (Fig. 3e). As a consequence, air temperature decreased mainly during the warmest hours of the day (that is, T_{max}), with statistically significant decreases from 12:00 to 17:00.

Evidence of how the glacier cooling effect influences the precipitation amount at high elevation is shown in Fig. 3f. We observe a higher daytime (9:00–17:00) precipitation amount at Pyramid$_{off}$, than at the stations at lower elevations. The same elevation pattern was reported for Mount Everest and Langtang Valley[20] and for Marsyandi Valley[23]. This is due to the local convergence between (cool, katabatic) down-valley and (warm, monsoonal) up-valley winds described in Fig. 2a.

https://doi.org/10.1038/s41561-023-01331-y

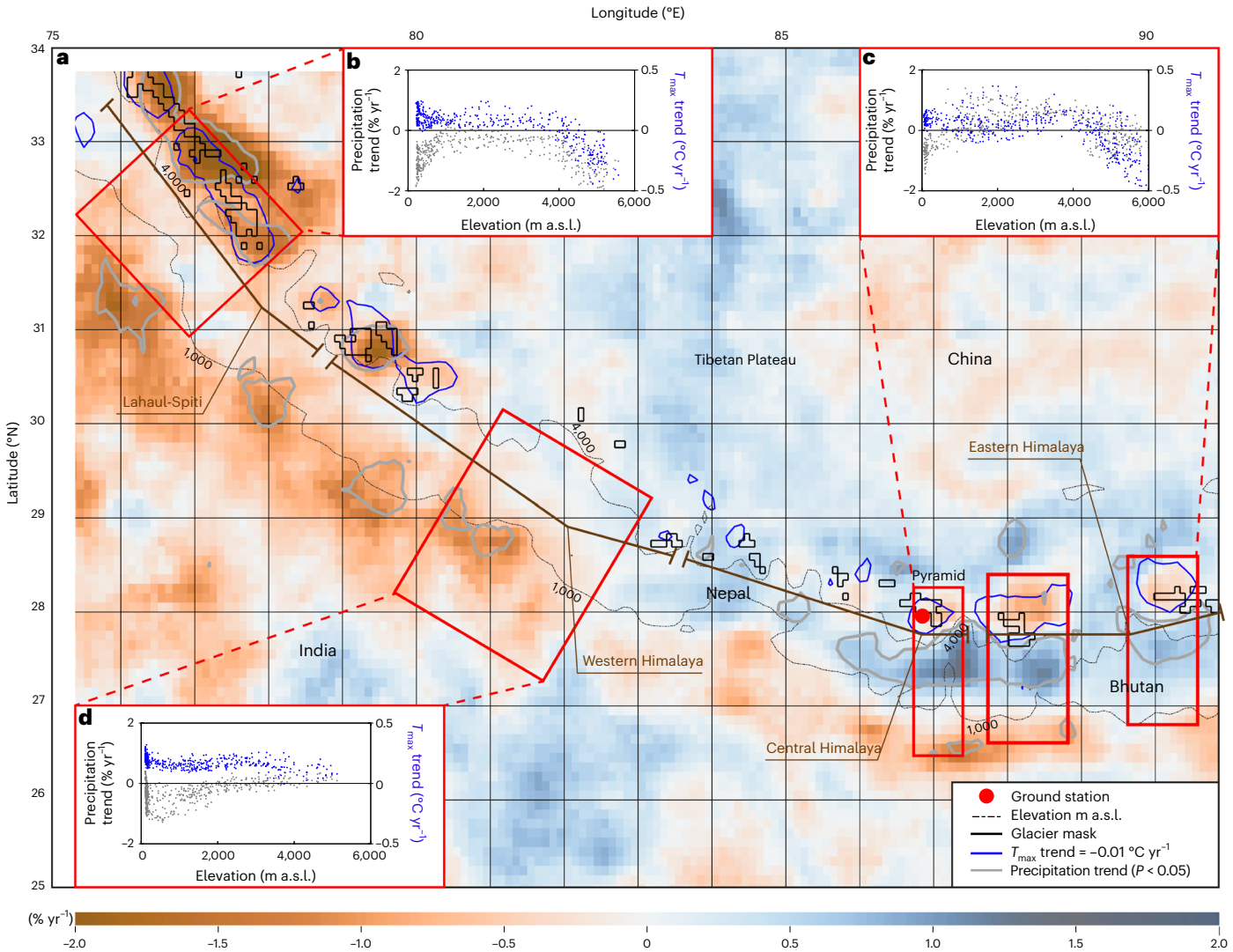

Fig. 4 | Himalayan trend of ERA5-Land diurnal (8:00–20:00) accumulated precipitation in the warm season (from May to October, during 1994–2020). **a**, The map reports the glacier mask used in ERA5-Land and the −0.01 °C yr^{-1} T_{max} cooling trend isolines (Fig. 1). Cold and warm colours represent decreasing and increasing precipitation trends (% yr^{-1}), respectively. The black line indicates their significance ($P < 0.05$). Three regions of interest have been selected to show the trend magnitudes for precipitation and temperature (from Fig. 1a) along the elevation gradient. **b**–**d**, The trend distribution is shown for Lahaul-Spiti (**b**), Western Himalaya (**c**) and Central-Eastern (**d**) subregions, respectively (blue points for precipitation trends, orange points for T_{max} trends). The same trend, but considering both diurnal and nocturnal precipitation, is reported in Supplementary Fig. 21.

Evidence of this process is provided by the substantial precipitation decrease (~50% with respect to the 1990s) at Pyramid$_{off}$ for all months of the warm season (−8.9 ± 5.0 mm yr^{-1}, $P < 0.001$, Supplementary Fig. 10a,b), during which 90% of the annual precipitation occurs[24]. The same decreasing trend was recorded at Pheriche$_{off}$ (Supplementary Fig. 4b), allowing one to exclude instrumental errors. ERA5-Land is able to reproduce the observed decreasing trends for some summer months (Supplementary Fig. 10c; Methods). Further evidence for the drying in the last decades stem from the evolution of high-elevated lakes; it was previously shown that possible variations in the lakes' evaporation have a decidedly lower relative importance than that of precipitation[25]. Indeed, lakes fed only by precipitation show decreasing trends in area and volume from the mid-1990s both in the Mount Everest region[25] and in the southern Tibetan Plateau[26,27].

Across the entire Himalayan arc, the decreasing T_{max} trends (Fig. 4a) correspond significantly with decreasing diurnal precipitation trends ($P < 0.001$). In Lahaul-Spiti, diurnal precipitation is decreasing (Fig. 4b), as it is in Central-Eastern Himalaya, although with a reduced magnitude and crucially only at high elevation (Fig. 4c). In contrast, in West Nepal, where glacier masses are smaller and their effect on the local climate reduced, the pattern is stationary or slightly increasing (Fig. 4d). It is worth noting that, in both Western and Eastern Himalaya (where decreasing trends are found), trends present a lower magnitude or opposite direction at lower elevations. This further confirms that the drying at high elevation is not caused by changes in large-scale atmospheric circulations.

Modelling the cooling and drying

In the recent decades of global warming (Supplementary Fig. 11), ERA5 shows a positive trend in daytime wind speed of katabatic winds (Supplementary Fig. 12b,c) flowing north and south of the Himalayan chain close to the glacier masses. During warmer days, the glacier nodes of ERA5-Land show more negative air temperature gradients (Supplementary Fig. 13b), resulting in enhanced diurnal downslope density winds (Supplementary Fig. 12c), sustained by the steep orographic gradients of the Himalayan chain (Supplementary Fig. 14). The same causal link between increased air temperature and katabatic wind emerged from high-resolution atmospheric simulations (Supplementary Fig. 15b3).

As a result, a decrease in T_{max} is evident in the entire Himalayan region in correspondence to the glacier surfaces of ERA5-Land (Fig. 1a).

In stationary conditions, ERA5-Land shows drying below the glaciers in the afternoon hours concomitant to a negative meridional wind gradient (southerly flow) anomaly (Supplementary Fig. 13d). On the contrary, in non-stationary conditions, a key consequence of the cooling (Fig. 1a) induced by increased katabatic winds (Supplementary Fig. 12), is the decreasing of the diurnal precipitation trends across the entire Himalayan arc (Fig. 4a). This is suggested to be caused by a downshift of the local convergence between up- and down-valley winds, which causes drying conditions at glacier elevations. This hypothesis is supported by our high-resolution atmospheric simulations which show this downshift of the convergence front (Supplementary Fig. 15b3).

Implications for climate change impacts in the Himalayas

Our study has provided evidence for a hitherto missed process in glacier–climate interactions at high elevations. We have described a glacier effect on local climate in the Himalaya, associated with global warming, which has lowered the daytime temperature close to the glacier masses. Potentially, glacier effects on local temperature could occur in other mountain chains, where glaciers can develop katabatic winds according to local climate regime, glacier size, slope and debris cover[16,28].

The proposed conceptual model reconciles the apparent discrepancy between the observed local cooling and the accelerated glacier mass loss in Himalaya. While atmospheric warming is increasing glacier ablation, the lowering of the near-surface air temperature over the glacier surface and consequent enhancement of katabatic winds has shifted the extent of daytime cooling toward the lower reaches of the glaciers and into the proglacial domain. Whereas the local cooling could have partially protected these low glacier reaches from warming, it has further lowered the elevation of the local wind convergence and consequently precipitation has diminished at high elevation, implying a further negative effect on glacier mass balance. This precipitation decrease was proposed by ref. 29, after observing the glacier changes in the Mount Everest region over the last decades, although its relative impact is currently unknown.

In nearby periglacial areas, the effect we describe will have key implications as the decrease in air temperature has affected the elevation band between the mean elevation of glaciers (~5,400 m a.s.l.) (ref. 2) and the periglacial environment even below 4,500 m a.s.l (Fig. 1b). In those elevation bands, areas of permafrost may exist[30] and their reaction to warming may be moderated by local cooling and drying during the summer, which drives permafrost thaw and associated geomorphic effects and hazards[31] through increasingly deep seasonal thawing. Long-term observations for testing this hypothesis, however, are virtually absent[30] and our study provides a compelling motivation to collect more high-elevation, long-term data to prove the new findings and their broader impacts.

Increased cooling during the early warm season in periglacial areas has the potential to reduce snowmelt rates and lengthen the snow season. However, at $Pyramid_{off}$, snow cover is not affected by this local cooling since during the warm season the snow cover is almost absent, as T_{max} is largely positive at this elevation (Supplementary Fig. 16).

This phenomenon we discuss could substantially influence mountain ecosystems. It is well known that mountain plant species have shifted upslope in response to global warming. Unexpectedly, however, ref. 32 observed stable vegetation line elevation, reduction in greening (productivity loss) and decreasing recruitment during the last three decades in three glacierized areas in the Himalayas, providing a surprising, independent validation of our findings of local cooling and drying.

The process we highlighted is potentially of global relevance and may occur on any glacier worldwide where conditions are similar. We limited our analysis to the Himalaya, also considering the scarcity of data in high-elevation areas across the globe but future research should look into its existence in other regions of the world and into the morphological (for example, debris cover, local topography, total glacier area and glacier energy balance) and climatic factors that control it. Some of those elements have a simplified representation in ERA5-Land because of ERA5-Land coarse spatial resolution (or are absent, for example, debris cover). It is promising, however, that the reanalyses are able to represent the first-order controls and main processes leading to cooling and the generation of katabatic winds. Future research should focus on establishing the factors determining the occurrence, magnitude and downward effects of katabatic processes, the cooling they induce and their ability to change glacier mass balance across climates and regions.

Online content

Any methods, additional references, Nature Portfolio reporting summaries, source data, extended data, supplementary information, acknowledgements, peer review information; details of author contributions and competing interests; and statements of data and code availability are available at https://doi.org/10.1038/s41561-023-01331-y.

References

1. Biemans, H. et al. Importance of snow and glacier meltwater for agriculture on the Indo-Gangetic Plain. *Nat. Sustain.* **2**, 594–601 (2019).
2. Bolch, T. et al. in *The Hindu Kush Himalaya Assessment* (ed. Wester, P. et al.) 209–255 (Springer Nature, 2019).
3. King, O. et al. Six decades of glacier mass changes around Mt. Everest area revealed by historical and contemporary images. *One Earth* **3**, 608–620 (2020).
4. Yao, T. et al. The imbalance of the Asian water tower. *Nat. Rev. Earth Environ.* **3**, 618–632 (2022).
5. IPCC. *Special Report on the Ocean and Cryosphere in a Changing Climate* (eds Pörtner, H.-O. et al.) (IPCC, 2020).
6. Pepin, N. et al. Elevation-dependent warming in mountain regions of the world. *Nat. Clim. Change* **5**, 424–430 (2015).
7. Thakuri, S. et al. Elevation-dependent warming of maximum air temperature in Nepal during 1976–2015. *Atmos. Res.* **228**, 261–269 (2019).
8. Maurer, J. M. et al. Acceleration of ice loss across the Himalayas over the past 40 years. *Sci. Adv.* **5**, eaav7266 (2019).
9. Guo, D. et al. Satellite data reveal southwestern Tibetan plateau cooling since 2001 due to snow–albedo feedback. *Int. J. Clim.* **40**, 1644–1655 (2020).
10. Huang, L. et al. Winter accumulation drives the spatial variations in glacier mass balance in High Mountain Asia. *Sci. Bull.* **67**, 1967–1970 (2022).
11. Sakai, A. Brief communication: updated GAMDAM glacier inventory over high-mountain Asia. *Cryosphere* **13**, 2043–2049 (2019).
12. Steiner, J. F. & Pellicciotti, F. Variability of air temperature over a debris-covered glacier in the Nepalese Himalaya. *Ann. Glaciol.* **57**, 295–307 (2016).
13. Greuell, W. & Böhm, R. 2m temperatures along melting mid-latitude glaciers and implications for the sensitivity of the mass balance to variations in temperature. *J. Glaciol.* **44**, 9–20 (1998).
14. Shea, J. M. & Moore, R. D. Prediction of spatially distributed regional-scale fields of air temperature and vapor pressure over mountain glaciers. *J. Geophys. Res. Atm.* **115**, D23107 (2010).
15. Carturan et al. Air temperature variability over three glaciers in the Ortles–Cevedale (Italian Alps): effects of glacier fragmentation, comparison of calculation methods and impacts on mass balance modeling. *Cryosphere* **9**, 1129–1146 (2015).
16. Shaw et al. Distributed summer air temperatures across mountain glaciers in the south-east Tibetan Plateau: temperature sensitivity and comparison with existing glacier datasets. *Cryosphere* **15**, 595–614 (2021).

17. Zhu, T. et al. Downward transport of ozone-rich air near Mt. Everest. *Geophys. Res. Lett.* **33**, L23809 (2006).
18. Ayala, A. et al. Modeling 2 m air temperatures over mountain glaciers: exploring the influence of katabatic cooling and external warming. *J. Geophys. Res. Atm.* **120**, 3139–3157 (2015).
19. Potter, E. R. et al. Dynamical drivers of the local wind regime in a Himalayan valley. *J. Geophys. Res. Atm.* **123**, 13–186 (2018).
20. Lin, C. et al. Summer afternoon precipitation associated with wind convergence near the Himalayan glacier fronts. *Atmos. Res.* **259**, 105658 (2021).
21. Cai, X. et al. Glacier winds in the Rongbuk Valley, north of Mount Everest. 2. Their role in vertical exchange processes. *J. Geophys. Res. Atm.* **112**, D11102 (2007).
22. Immerzeel, W. et al. The importance of observed gradients of air temperature and precipitation for modeling runoff from a glacierised watershed in the Nepalese Himalayas. *Water Resour. Res.* **50**, 2212–2226 (2014).
23. Barros, A. P. et al. A study of the 1999 monsoon rainfall in a mountainous region in central Nepal using TRMM products and rain gauge observations. *Geophys. Res. Lett.* **27**, 3683–3686 (2000).
24. Salerno, F. et al. Weak precipitation, warm winters and springs impact glaciers of south slopes of Mt. Everest (central Himalaya) in the last 2 decades (1994–2013). *Cryosphere* **9**, 1229–1247 (2015).
25. Salerno, F. et al. Glacier melting and precipitation trends detected by surface area changes in Himalayan ponds. *Cryosphere* **10**, 1433–1448 (2016).
26. Jiang, L. et al. Monitoring recent lake level variations on the Tibetan Plateau using CryoSat-2 SARIn mode data. *J. Hydrol.* **544**, 109–124 (2017).
27. Zhang, G. et al. Response of Tibetan Plateau lakes to climate change: trends, patterns and mechanisms. *Earth Sci. Rev.* **208**, 103269 (2020).
28. Potter, E. R. et al. Meteorological impacts of a novel debris-covered glacier category in a regional climate model across a Himalayan catchment. *Atmos. Sci. Lett.* **22**, e1018 (2021).
29. Thakuri, S. et al. Tracing glacier changes since the 1960s on the south slope of Mt. Everest (central Southern Himalaya) using optical satellite imagery. *Cryosphere* **8**, 1297–1315 (2014).
30. Gruber, S. et al. Inferring permafrost and permafrost thaw in the mountains of the Hindu Kush Himalaya region. *Cryosphere* **11**, 81–99 (2017).
31. Deline, P. et al. in *Snow and Ice-related Hazards, Risks and Disasters* (eds Haeberli, W. & Whiteman, C.) 501–540 (Elsevier, 2021).
32. Sigdel et al. No benefits from warming even for subnival vegetation in the Himalayas. *Sci. Bull.* **66**, 1825–1829 (2021).

Methods

Region of investigation and climate

The ground meteorological network belongs to the Pyramid Network[24], which is located on the southern side of Mount Everest along the Khumbu Valley, central Himalaya. The land-cover classification shows that almost one-third of the territory is characterized by glaciers and ice cover, while less than 10% of the area is forested. Glacial surfaces are distributed from 4,300 to above 8,000 m a.s.l. These glaciers are identified as the summer-accumulation type, which are fed mainly by summer monsoon precipitation[33]. The climate in the South Asia and Himalayan region has a strong annual cycle, with the South Asian monsoon as a phase of this annual cycle. Regarding precipitation, the 20 yr measurements at $Pyramid_{off}$ show that 90% occurs from June to September, while the probability of snowfall during these months is very low (4%). The annual cumulative precipitation at this elevation is 446 mm, with a mean annual temperature of −2.5 °C. The relatively low annual precipitation at this elevation is due to the elevation-dependent depletion of the moisture content resulting in a severe reduction of precipitation at higher elevations[24].

As we show in Fig. 3 (ref. 34), in agreement with other authors[35], the nocturnal maximum precipitation peak occurs most strongly during the summer monsoon. Furthermore, ref. 35 noted an asymmetry in diurnal winds, with daytime up-valley winds strongly predominating over weak nocturnal down-valley flow, with the daytime asymmetry being strongest during the monsoon.

A previous study[36] has also documented the enhancement of nocturnal katabatic winds in the warm season over the Himalaya in recent decades (1979–2014), attributed to nocturnal clearer skies, which radiatively cooled the slopes, enhancing downslope winds.

We checked the possible relationship between the Interdecadal Pacific Oscillation[37] and T_{max} trend at $Pyramid_{off}$ during the warm season (1994–2020). We did not find any significant relationship, although both series were decreasing in the last decades, thus excluding any possible influence from large-scale variability on the T_{max} trend observed at $Pyramid_{off}$.

High-elevation climatic data (Nepal). The first station ($Pyramid_{off}$) was established near the Pyramid Observatory Laboratory (5,035 m a.s.l.) in 1994. The main meteorological parameters (temperature, precipitation, relative humidity and wind) are recorded continuously (on an hourly basis), representing the longest time series existing at the high Himalayan elevations. Extra Automatic Weather Stations (AWSs) were installed along the Khumbu Valley in the following years. Metadata and location map are provided in Supplementary Table 3 and Supplementary Fig. 1. Wind, air temperature and precipitation sensors used in this study were supplied by LSI-Lastem (https://www.lsi-lastem.com/). All instrument details can be downloaded from http://geonetwork.evk2cnr.org.

$Namche_{off}$ station (3,560 m a.s.l.) is located in a forest-dominated landscape, $Pheriche_{off}$ (4,260 m a.s.l.) is slightly above the treeline (alpine tundra), $Pyramid_{off}$ (5,035 m a.s.l.) is located at the mean elevation of glacial fronts[33]. The $Changri_{on}$ is a station located on the Changri-Nup Glacier (5,700 m a.s.l.) and is used in this study to investigate the relationship between katabatic winds and the glacier cooling effect. The Changri-Nup is a debris-covered glacier with a southeastern aspect (total length of ~4 km and a total area of ~2.7 km^2). The accumulation zone of the glacier is a cirque surrounded by peaks reaching elevations >6,500 m a.s.l. Most of the ablation zone is covered by debris interspersed with supraglacial ponds and ice cliffs. The debris-covered portion of the tongue has a length of 2.3 km and an average width of 0.7 km, with a terminus located at 5,240 m a.s.l. Meteorological parameters were continuously monitored from 2011 to 2015, using an AWS installed on the debris-free surface of the glacier at 5,700 m a.s.l. AWS data were measured at 60 s intervals and averaged over a 30 min time period.

Data processing. We performed the data processing and quality checks according to the international standards of the World Meteorological Organization. The precipitation at all stations was measured using conventional buckets. Therefore, we only analysed the data collected in the warm season. Data discontinuity (for different variables) often occurred due to logistical problems at these elevations.

Data gap filling for temperature and precipitation time series. $Pyramid_{off}$ has suffered a percentage of missing daily values of ~10% over the last 27 years, for both temperature and precipitation. In this study, we apply the same filling method (mainly quantile mapping) used for missing data in ref. 24 but extending the time series to 2020. The uncertainty introduced by the filling process on the Sen's slope (SS) was estimated through a Monte Carlo uncertainty analysis[24].

Low-elevation climatic data (Nepal). Meteorological data in Nepal are collected and managed by the Department of Hydrology and Meteorology, Government of Nepal. We used daily T_{max} and precipitation data series (1994–2020) covering an elevation range between 0 and 2,000 m a.s.l. Among these stations, we selected only stations with few missing data (<10%). The selected stations are homogeneously distributed in the country (Supplementary Fig. 17). The comparison with ERA5-Land data has been made considering 27 T_{max} and 157 precipitation stations (Supplementary Figs. 8 and 18, respectively).

High-elevation climatic data (Tibetan Plateau). The Chinese station data are provided by the China Meteorological Administration. The three stations close to the glacier masses have been recently discussed in ref. 9 (Nielaer, Pulan and Shiquanhe). The remaining two stations (Dingri and Gaize), located farther from glaciers, are used for comparison. Supplementary Table 1 provides some technical details on the stations, percentage of glacier cover included in a 20 km radius and minimum distance from the glacier fronts to each station. Supplementary Fig. 9 shows the relationship (distance and glacier cover) between those stations and the glacier masses. Trends analysis is shown in Supplementary Fig. 5.

Ozone data at high elevation (Nepal). The Nepal Climate Observatory-Pyramid (NCO-P, 27° 57′ N, 86° 48′ E) is located at 5,079 m a.s.l., a few metres from $Pyramid_{off}$. As shown by ref. 38, the air-mass circulation at this measurement site is strongly influenced both by the synoptic scale circulation and the local mountain wind regime. The interaction between these components leads to the onset and decay of the summer monsoon and winter seasons[38]. At NCO-P, ozone-rich air masses indicate transport from the upper atmosphere[39]. Surface O_3 measurements have been continuously performed over 2006–2015 with a UV-photometric analyser (Thermo Scientific, Tei 49C). During a maintenance campaign in February 2007, the instrument was compared against a travelling standard by GAW/WCC at EMPA (World Calibration Centre for Surface Ozone, Carbon Monoxide and Methane at the Swiss Federal Laboratories for Materials Testing and Research). The combined standard uncertainty (1 min basis) was ascertained to be less than ±1.5 ppbv in the range 0–100 ppbv.

The three classes of hourly wind speed at $Changri_{on}$ station (warm season) described in Fig. 3c were defined on the basis of the following criteria: wind direction between 90° and 270° (southward) and wind speed >1 m s^{-1}. When one of the two criteria was not satisfied, we included the observations in the 'no event' class. The significance of the differences among the three classes was evaluated using the Dunn's Kruskal–Wallis test (post hoc test for non-parametric comparison)[40].

ERA5-Land reanalysis data. At present, among the reanalysis products with a high spatial resolution, there are three main products: ERA5-Land[41] and two dynamical downscaling products. ERA5-Land is a reanalysis product derived by running the land component of

ERA5 at increased resolution, which is enhanced globally to 9 km (0.1°) compared to 31 km (0.25°) (ERA5) or 80 km (0.70°) (ERA-Interim), whereas the temporal resolution is hourly and the simulations cover from 1950 to the present as in ERA5 (ref. 41). High Asia Reanalysis v.2 is a 10 km resolution dynamical downscaling of ERA5 performed using the Weather Research and Forecasting (WRF) model at present only available from 2004[42]. Another dynamical downscaling is a 6.7 km resolution product derived by Climate Forecast System Reanalysis data using the WRF model[36] available until 2014. These last two high-resolution dynamical downscaling products might have potentially improved the spatial representation of mountain precipitation; however, currently, they do not cover the entire period considered in this study. Therefore, we considered T and P data from the state-of-the-art ERA5-Land gridded climate reanalysis.

ERA5-Land is driven by atmospheric forcing derived from ERA5 near-surface meteorology state and flux fields. The meteorological state fields are obtained from the lowest ERA5 model level (level 137) and include air temperature, specific humidity, wind speed and surface pressure. The 2 m air temperature in ERA5-Land is a diagnostic output similar to ERA5 forecasts; that is, it is calculated with 10 m air temperature from ERA5 and the heat flux from ERA5-Land according to the Monin–Obukhov similarity theory. The surface fluxes include downward shortwave and longwave radiation and liquid and solid total precipitation. These fields are interpolated from the ERA5 resolution of about 31 km to ERA5-Land resolution of about 9 km using a linear interpolation method based on a triangular mesh.

In this regard, the Himalayan trends of ERA5 and ERA5-Land for T_{max} were explored here considering the same analysis period (warm season during 1994–2020). We found that the decreasing pattern diagnosed by the two products (Fig. 1a and Supplementary Fig. 19 for ERA5-Land and ERA5, respectively) is the same even if ERA5 is characterized by a lower spatial resolution.

Moreover, we compared T_{max} observed at the Pyramid$_{off}$ and the corresponding ERA5-Land data in terms of correlation (Supplementary Fig. 20a) and bias (Supplementary Fig. 20b). Generally, the uncertainty of this reanalysis product was found to be low for all months of the year. Particularly, the bias results are constant for all considered years. This means that the non-stationarity is not influenced by possible biases during the analysed period.

Finally, ERA5-Land cannot be tested extensively at high elevations because of the lack of ground observations, while this is possible below 2,000 m a.s.l. for the entire area of Nepal. Therefore, we compared ERA5-Land with 157 ground stations (1994–2020 period). The relevant precipitation trends show good agreement (Supplementary Fig. 18).

Treatment of glaciers. Particularly important in this study is the representation in ERA5-Land of glaciers. As reported in ref. 41, the model formulation (as in ERA5) does not have an independent treatment of glaciers. Grid points with glaciers are assigned with a constant snow mass of 10 m. A threshold of 50% of a grid box covered by ice is used, below which the snow depth keeps the value computed by the snow scheme of the land model. Values above the threshold assign a snow water equivalent value of 10 m. This condition is used to avoid grid points near glaciers with large unrealistic snow depth that result from the interpolation from ERA5 fields to ERA5-Land[41].

Precipitation and temperature. Currently, ERA5 is the most accurate of the existing reanalysis products for precipitation detection[43]. Others[44] reviewed some recent studies showing the capability of ERA5 (both for temperature and precipitation) in complex terrain such as High Mountain Asia, where in situ meteorological observations are sparse and unevenly distributed. Among these studies, the performance of ERA5 precipitation over High Mountain Asia was analysed by ref. 45 and ref. 46. They found that ERA5 succeeds in reproducing the interannual and decadal variabilities of precipitation and reflecting the spatiotemporal patterns of precipitation over the whole Tibetan Plateau. Considering the temperature trends in mountains, recent studies, devoted to the comparison of different reanalysis products, point out that ERA5 performs well in capturing the non-stationarity of temperature during last decades on the Tibetan Plateau[47].

In this study, a similar comparison was carried out in Nepal at low elevations (<2,000 m a.s.l.) for T_{max} and precipitation (Supplementary Figs. 8 and 15, respectively). All these results provide robust evidence about the capability of ERA5 to correctly describe the large-scale trends. Regarding the high Himalayan elevations, Pyramid$_{off}$ data have never been assimilated into ERA5 and this has not occurred for other high-elevated stations as well, considering their general absence at these elevations. Thus, any possible problem related to changes in station density or location over time should not have affected the local climatic trends. Therefore, Pyramid$_{off}$ data are used here for validating the capability of ERA5-Land to simulate the non-stationarity of precipitation and temperature at the local level.

Trends analysis: the sequential Mann–Kendall test. In this study, the Mann–Kendall test (MK) was applied at the monthly scale (after daily data aggregation) to analyse the non-stationarity of observational and reanalysis data. This test is widely adopted to assess significant trends in hydrometeorological time series[48]. This test is non-parametric, thus being less sensitive to extreme sample values and is independent from the hypothesis about the nature of the trend, whether linear or not. The MK test verifies the assumption of the stationarity of the investigated series by ensuring that the associated normalized Kendall's tau-b coefficient[48], $\mu(\tau)$, is included within the confidence interval for a given significance level (for $\alpha = 5\%$, the $\mu(\tau)$ is below −1.96 and above 1.96). We used the SS proposed by ref. 49 as a robust linear regression allowing the quantification of the potential trends revealed by the MK. The significance level is established for $P < 0.05$. We defined a slight significance for $P < 0.10$. The uncertainty associated with the SS (1994–2013) is estimated through a Monte Carlo uncertainty analysis. Further details on this uncertainty are reported in ref. 24. In the sequential form (seqMK) $\mu(\tau)$ the test is applied forward starting from the oldest values (progressive trend) and backward starting from the most recent values (retrograde trend). The crossing period allows us to identify the approximate starting point of the trend.

Data availability

The meteorological data from the Pyramid Observatory Laboratory are available at http://95.110.144.131/geoportal/data/search. The ozone data are available at the World Data Centre for Reactive Gases (GAW-WDCRG) and accessible at the EBAS data infrastructure hosted by NILU (http://ebas.nilu.no). Meteorological fields from ERA5-Land reanalysis data used in this study are available from the Copernicus Climate Data Store at https://cds.climate.copernicus.eu/cdsapp#!/dataset/reanalysis-era5-land?tab=form. The ground station data for Nepal are obtained from the Department of Hydrology and Meteorology, Nepal, and can be requested at http://www.dhm.gov.np. The temperature data for the Chinese stations are obtained from the National Meteorological Information Center (http://data.cma.cn/). Source data are provided with this paper.

Code availability

Data processing techniques are available on request from F.S. and N.G. (franco.salerno@cnr.it; nicolas.guyennon@irsa.cnr.it).

References

33. Salerno, F. et al. Debris-covered glacier anomaly? Morphological factors controlling changes in the mass balance, surface area, terminus position and snow line altitude of Himalayan glaciers. *Earth Planet. Sci. Lett.* **471**, 19–31 (2017).

34. Ueno, K. et al. Meteorological observations during 1994–2000 at the Automatic Weather Station (GEN-AWS) in Khumbu region, Nepal Himalayas. *Bull. Glaciol. Res.* **18**, 23–30 (2001).
35. Barros, A. P. & Lang, T. J. Monitoring the monsoon in the Himalayas: observations in central Nepal, June 2001. *Mon. Weather Rev.* **131**, 1408–1427 (2003).
36. Norris, J. et al. Warming and drying over the central Himalaya caused by an amplification of local mountain circulation. *npj Clim. Atmos. Sci.* **3**, 1 (2020).
37. Chinta, V. et al. Influence of the Interdecadal Pacific Oscillation on South Asian and East Asian summer monsoon rainfall in CMIP6 models. *Clim. Dynam.* **58**, 1791–1809 (2022).
38. Bonasoni, P. et al. Atmospheric brown clouds in the Himalayas: first two years of continuous observations at the Nepal Climate Observatory-Pyramid (5079 m). *Atmos. Chem. Phys.* **10**, 7515–7531 (2010).
39. Cristofanelli, P. et al. Tropospheric ozone variations at the Nepal Climate Observatory-Pyramid (Himalayas, 5079 m a.s.l.) and influence of deep stratospheric intrusion events. *Atmos. Chem. Phys.* **10**, 6537–6549 (2010).
40. Dinno, A. Nonparametric pairwise multiple comparisons in independent groups using Dunn's test. *Stata J.* **15**, 292–300 (2015).
41. Muñoz-Sabater, J. et al. ERA5-Land: a state-of-the-art global reanalysis dataset for land applications.*Earth Syst. Sci. Data* **13**, 4349–4383 (2021).
42. Wang, X. et al. WRF-based dynamical downscaling of ERA5 reanalysis data for High Mountain Asia: towards a new version of the High Asia Refined analysis. *Int. J. Climatol.* **41**, 743–762 (2021).
43. Kraaijenbrink, P. D. et al. Climate change decisive for Asia's snow meltwater supply. *Nat. Clim. Change* **11**, 591–597 (2021).
44. Khanal, S. et al. Historical climate trends over High Mountain Asia Derived from ERA5 reanalysis data. *J. Appl. Meteorol. Climatol.* **62**, 263–288 (2023).
45. Sun, H. et al. General overestimation of ERA5 precipitation in flow simulations for High Mountain Asia basins. *Environ. Res. Comm.* **3**, 121003 (2021).
46. Yuan, X. et al. Characterizing the features of precipitation for the Tibetan Plateau among four gridded datasets: detection accuracy and spatio-temporal variabilities. *Atmos. Res.* **264**, 105875 (2021).
47. Huai, B. et al. Evaluation of the near-surface climate of the recent global atmospheric reanalysis for Qilian Mountains, Qinghai-Tibet Plateau. *Atmos. Res.* **250**, 105401 (2021).
48. Guyennon, N. et al. Benefits from using combined dynamical-statistical downscaling approaches—lessons from a case study in the Mediterranean region. *Hydrol. Earth Syst. Sci.* **17**, 705–720 (2013).
49. Sen, P. K. Estimates of the regression coefficient based on Kendall's tau. *J. Am. Stat. Assoc.* **63**, 1379–1389 (1968).

Acknowledgements

This work was carried out within the framework of the EV-K2-CNR and Nepal Academy of Science and Technology. K.Y. was supported by the Second Tibetan Plateau Scientific Expedition and Research Program (grant no. 2019QZKK0206). N.C. was supported by the project NODES, which has received funding from the MUR–M4C2 1.5 of PNRR funded by the European Union - NextGeneration EU (Grant agreement no. ECS00000036). T.E.S. has received funding from the European Union's Horizon 2020 research and innovation programme under the Marie Sklodowska-Curie grant no. 101026058. F.P. has received funding from the European Research Council under the European Union's Horizon 2020 research and innovation programme grant no. 772751, RAVEN, 'Rapid mass losses of debris-covered glaciers in High Mountain Asia' and has been supported by the SNSF grant 'High-elevation precipitation in High Mountain Asia' (grant no. 183633). A.A. was supported by the European Union's Horizon 2020 research and innovation program under grant agreement no. 101004156 (CONFESS project) and by the European Union's Horizon Europe research and innovation program under grant agreement no. 101081193 (OptimESM project). We thank H. Wehrli for valuable comments and suggestions and J. Giannitrapani for the graphic support. We thank A. Da Polenza and K. Bista of EV-K2-CNR for believing that studying the high elevations is relevant for the whole globe.

Author contributions

F.S. and N.G. conceived the idea of the research and equally contributed to this article. F.S., F.P. and N.C. drafted the article. F.S., N.G., K.Y. and A.A. developed the conceptual model. C.L. and K.Y. conducted the analysis for the WRF model. P.C. and D.P. conducted the analysis for ozone. G.B. provided the knowledge of physical processes of ERA5-Land. N.G., F.S., S.T. and N.C. prepared the figures. G.V. and G.T. provided the meteorological data and assured their quality. F.P., E.M., T.E.S., S.G., T.B., N.C., S.T., E.R., G.T. and G.D. contributed to improving the manuscript.

Competing interests

The authors declare no competing interests.

Additional information

Supplementary information The online version contains supplementary material available at https://doi.org/10.1038/s41561-023-01331-y.

Correspondence and requests for materials should be addressed to Franco Salerno or Nicolas Guyennon.

Peer review information *Nature Geoscience* thanks Jesse Norris and the other, anonymous, reviewer(s) for their contribution to the peer review of this work. Primary Handling Editor: Tom Richardson, in collaboration with the *Nature Geoscience* team.